

Landslides (2018) 15:565–580
 DOI 10.1007/s10346-018-0946-8
 Received: 1 June 2017
 Accepted: 4 January 2018
 Published online: 12 January 2018
 © Springer-Verlag GmbH Germany,
 part of Springer Nature 2018

Ming-liang Chen · Peng-fei Lv · Shi-lin Zhang · Xing-ze Chen · Jia-wen Zhou

Time evolution and spatial accumulation of progressive failure for Xinhua slope in the Dagangshan reservoir, Southwest China

Abstract This paper presents a preliminary study of time evolution and spatial accumulation of progressive failure for ancient landslide deposits in Xinhua slope. According to the geological response after impoundment, the Xinhua slope has shown the spatial accumulation of deformation, such as ground cracks in the rear edge, toe collapse, local shallow slides in intense rainfall, and progressive creep displacement. Approximately 2 years of monitoring was performed for the Xinhua slope with the assistance of the global navigation satellite system (GNSS), unmanned aerial vehicles (UAVs), and field investigations. The deformation process of a reservoir landslide is considered to be a comprehensive and complicated combination of geological influence from various adverse factors. Field investigations and monitoring indicate that the major serious influence after completion of dam construction comes from the initial large-scale impoundment, the fluctuation of water level, and the existence of a flood season. The creep/slip deformation of slope deposits is a result of integration with adverse hydraulic conditions, e.g., strong rainfall, intense currents and transient seepage flow inside the slope deposits, and activation by water level fluctuation, which can be verified from the twofold evident deformation in the flood season. For the reservoir with daily regulation ability, the occurrence of evident deformations in July highlights that the regulation plan for water level in the flood season is important for controlling the deformation of slope deposits, where the fluctuation of the water level is no more than 10 m in the operation period.

Keywords Reservoir landslides · Ancient landslide deposits · Response and evolution mechanism · Time evolution · Spatial accumulation

Introduction

With the development of society and economy, there are plenty of hydropower stations that have been built or are being built in Southwest China with the construction of high dams and large reservoirs. Due to the widespread distribution of slope deposits, strong weathering, and unloading of the shallow slope rock masses, reservoir landslide has become a very serious problem for the normal operation of hydropower stations in Southwest China (Wang and Li 2009; Zhou et al. 2010). In general, reservoir landslide is a typical geological failure occurred on a slope that is sensitive to hydraulic condition changes that are developed from the actions of reservoir impoundment, rainfall, manmade disturbance, strong earthquakes, and other triggering factors. They may block the roads, create landslide dams, bury the residential houses, and cause landslide-generated wave and others, posing a great threat to human lives, lifeline facilities, and natural environment (Zhou et al. 2010; Duc 2013; Dufresne et al. 2015; Xia et al. 2015; Zhou et al. 2016, 2017). This type of hazard is unpredictable and uncontrollable, which is considered to be a long-term accumulation of slope deformation (Saito et al. 2001; Wang et al. 2013).

Reservoir landslides can originate in slope deposits (e.g., ancient landslide deposits, weathered deposits, and quaternary glacial deposits) and/or soft broken rock mass with poor rock quality (e.g., fractured rock mass, soft rock mass, and existence of a weak interlayer), which are all sensitive to the water behavior from rainfall infiltration or reservoir impoundment (Iverson 2000; Berilgen 2007; Zhao et al. 2015). The influence of water on reservoir slopes can be mainly categorized into two aspects. The first aspect is the reduction of shear strength for rock/soil due to the softening effect from long-term immersion in water. The other aspect is the variation of pore water pressure and hydrodynamic force due to the fluctuation of water level, which increases the probability of large deformation, failures, or even catastrophic landslides in the reservoir slope (Yamada et al. 2013; Huang et al. 2015; Zhou et al. 2016).

For reservoir landslide, the present studies are primarily focused on the characteristics of slope deformation, the mechanism of landslide formation, and the risk analyses (Schwab et al. 2004; Tiwari and Lewis 2014). Field investigations, physical modeling tests, numerical simulations, and monitoring data analyses are the commonly used approaches for dealing with the related problems of reservoir landslides (Chelli et al. 2006; Xia et al. 2013; Yang and Wang 2014; Okeke and Wang 2016; Fan et al. 2017). The field investigation is used to obtain the geological identification and morphological cognition of landslide, and it is also the foundation work for the other three methods. Recently, some new remote sensing techniques are used to assist field investigations, such as unmanned aerial vehicles (UAVs) and three-dimensional (3D) laser scanning (Casagli et al. 2017a, 2017b). The physical modeling and numerical simulation are both well-known for understanding the behavior of landslides through quantitative analyses. However, both approaches have difficulty in making a truthful and accurate reproduction of the whole process of slope failure (Panizzo et al. 2005; Wang and Li 2009). Meanwhile, the difficulty is also the breakthrough direction for the development of these two methods (Wang et al. 2013). The monitoring data analysis is achieved by real-time tools for recording the deformation of a targeted landslide, such as the global navigation satellite system (GNSS) (Shi et al. 2015; Chelli et al. 2006). These different methods are all used to understand the internal physical mechanisms and dynamic processes of reservoir landslides that can help us formulate effective hazard prevention and mitigation measures and reduce disaster impacts and losses (Bjerrum 1967; Bansal and Das 2011; Vandamme and Zou 2013; Hungr et al. 2014). The investigation, analysis, evaluation, and prediction of slope deposits with potential geological hazards are of great importance for the following considerations: (1) acquiring the distribution and surface morphology characteristics of slope deposits for a sufficient qualitative and quantitative understanding; (2) making a correct description (e.g., initiation and propagation time, slope displacement,

direction, and velocity) and interpreting the movement pattern and evolution mechanisms of landslides from the monitoring data; and (3) how to evaluate slope stability and potential hazards based on the characteristics of slope deformation in consideration of the influencing factors (e.g., rainfall, impoundment, and earthquake).

The studied site Dagangshan Hydropower Station started impoundment in May 2015, and the water level has continuously risen since then, resulting in the inundation of a large mountainous area. Meanwhile, the water level often fluctuates due to the operation of the hydropower station, which has caused large deformations, failures, and even landslides in several reservoir slopes. These problems of reservoir landslides and/or large deformation of slopes pose a great threat to the nearby lifeline facilities and the normal operation of the hydropower station. With different formation processes, geological distribution, and activity, a number of reservoir slope failures in this area have resulted in complex evolutions of landform geologic partitioning, lithology, and hydrology (Chelli et al. 2006). The Xinhua slope is a typical geological disaster in the Dagangshan reservoir that has large deformation, surface cracking, and local failures. In case of a potential catastrophic large landslide initiated on this slope, it will generate the following hazardous consequences: (a) interruption of the mountain road connected with the Xinhua village, (b) possible harm to the personnel near the Xinhua slope, and (c) interruption of provincial road S211 on the opposite bank with the action of a landslide-generated wave.

In this paper, the Xinhua slope with large deformations and failures after the impoundment of Dagangshan reservoir is taken as an example to study the evolution and spatial accumulation of slope progressive failure. The research consists of field investigation and monitoring data analysis with the assistance of the GNSS, geological boreholes, and UAV device. The geological conditions and slope material properties are analyzed by field investigation and UAV device. Then, qualitative analyses for the evolution of cumulative deformation and cracks in the slope are performed based on field investigation and site monitoring data. Finally, the formation and evolution mechanisms of the progressive failure of Xinhua slope are discussed, and several useful conclusions about the slope response for rainfall and variation of water level are presented for understanding the progressive failure of reservoir bank slopes.

Geological and geomorphological setting

Landforms

The Xinhua slope is located in the Xinhua Village (E102° 10' 51.20", N29° 29' 57.49"), Detuo Town, Sichuan Province (Fig. 1a), characterized by an ancient landslide deposit with the potential for reactivation. It is in the upstream of Dagangshan reservoir on the left bank of the Dadu River and is approximately 14.6 km from the dam site of the Dagangshan Hydropower Station (Fig. 1b). The slope deposits cover an area of 0.27 km² with an estimated volume of 7.0×10^6 m³. The slope surface topography is shaped similar to a round-backed armchair with a length of 600 m, a width of 450 m, and a thickness of slope deposits of approximately 50–70 m. There is a shallow gully in the middle part developed with the same direction as the slope distribution.

The Xinhua slope extends from the front elevation of 1065 m to the rear elevation of 1420 m along a direction orthogonal to the flow direction of the Dadu River, and the designed normal water level is the elevation of 1130 m. The slope toe was approximately 35 m above the water level before reservoir impoundment, but the lower slope was submerged into the water after reservoir impoundment. The slope has an upper part of flat topography without sag area but a steep front edge, where the elevation from 1070 to 1300 m has a general gradient approximately 30°–40°, and the gradient for the elevation from 1300 to 1420 m is approximately 14°–24°. In addition, the frontal edge of the slope has a free face, caused by road excavation and suffering persistent impact of current scouring after impoundment. There is a high potential of the occurrence of landslides on the Xinhua slope, which may produce an adverse impact on the operation of the Dagangshan Hydropower Station and the danger for personnel and assets on the slope.

Geological framework

The Xinhua slope can be divided into three geological partitions according to the geologic conditions and deformation characteristics: a relative stable region (C) situated at the slope rear edge and two regions arranged side by side at the lower slope (as shown in Fig. 2). The west region (B) and the east region (A) constitute the main body of the Xinhua slope, and it is characterized by a dark gray rubble soil layer with the petrographic composition of

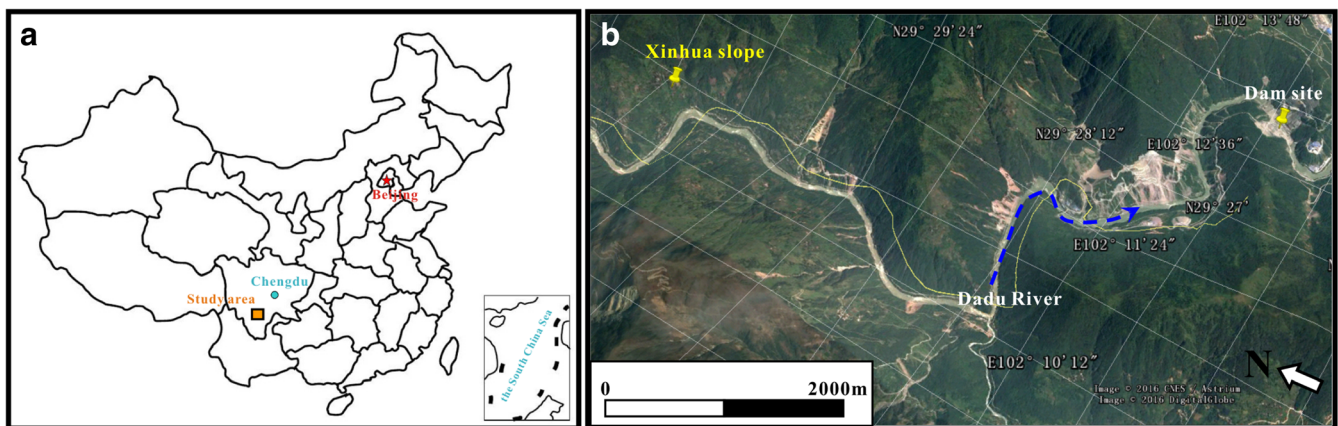


Fig. 1 Location and terrain of the study area: a site location of the study area and b topographic and geomorphic features of the Dagangshan reservoir (from Google Earth, 2017)

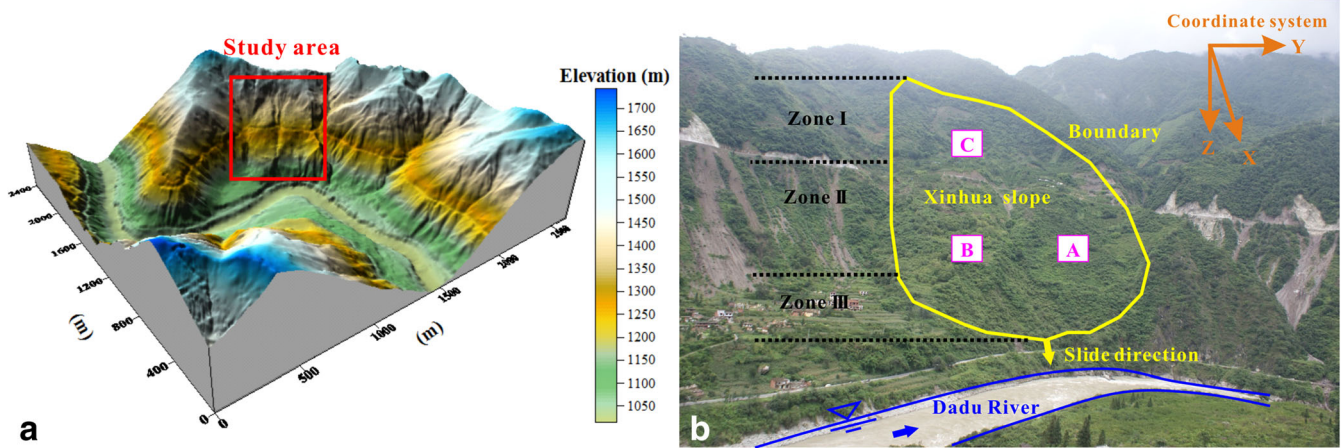


Fig. 2 Topographic characteristics of the Xinhua slope: **a** three-dimensional visualization of the study area and **b** overall view of the Xinhua slope (three subregions can be divided for the slope)

sandstone. Rock blocks amount to 10%, the crushed rock and/or rock fragments amount to 50%, and the silty clay amounts to 40%. The slope region C is characterized by a light slope wash layer with petrographic composition of granite and diorite. The mass percentage of rock blocks, rock fragments, gravel stone, and silty clay amount to 5, 30, 40, and 25%, respectively. Table 1 summarizes the thickness of the slope deposits revealed by the site borehole results. The overburden thickness of the slope deposits is in the range from 40 to 100 m in different locations, and the average overburden thickness is approximately 65–70 m (Fig. 3).

According to the exposure from several boreholes in the slope, the slope deposits can be divided into three subzones according to the contact situation with underlying strata and the development characteristics of the slip band: zone I (rear traction section), zone II (middle major slipping section), and zone III (lower slipping nappe section). The soil of the slip band in deep stratum is characterized by dark gray silty clay with gravel, which grows in zone II with thickness primarily from 0.55 to 6.41 m, and a maximum thickness of 18.42 m (Dx07, as shown in Fig. 3b). However, there is almost no development in the slip band of zone I and zone III (Dx03 and Dx04, as shown in Fig. 3b and c). The main composition of gravel is sandstone subangular particles. Meanwhile, the

boreholes Dx06 and Dx07 discovered two slip bands in the shallow zone indicating that slip movement was initiated there.

Lithology

The lithological characteristics and structural form in the study area have been studied through the boreholes and field investigations. Figure 4 shows the typical geological conditions of the Xinhua slope. The Xinhua slope is mainly composed of quaternary accumulations, including ancient landslide deposits, and weathered and alluvial deposits (Fig. 4a and b). Table 2 shows the mechanical properties of slope deposits in different zones. Strong weathered and fractured rock masses are exposed at the slope edge and the lower part below the deposits (Fig. 4c and d), but not the main component. As shown in Fig. 3a, the bedrock exposed in the reservoir area is characterized by sandstone and shale of the Baiguowan group of the Triassic system (T_{3bg}) with soft lithology and low rock strength. The attitude of rock formation is characterized by a strike angle of $N0^{\circ}-10^{\circ}E$, a dip direction of NWW and a dip angle of $46^{\circ}-70^{\circ}$. Around the slope deposits, the upstream side is characterized by quartz diorite ($\delta_{O_2}^3$), and the downstream side is characterized by medium-grained biotite adamellite ($\gamma_{O_2}^2$ and $\gamma_{K_2}^2$). The alluvium, covered by the front edge of slope

Table 1 Thickness of the slope deposits revealed by the site borehole results

No.	Hole elevation (m)	Hole depth (m)	Overburden thickness (m)
Dx01	1363.02	80.80	57.95
Dx02	1191.18	105.00	80.90
Dx03	1080.88	48.50	42.85
Dx04	1361.87	80.10	53.95
Dx05	1169.04	83.50	63.85
Dx06	1139.08	85.73	62.78
Dx07	1319.96	120.12	98.50
Dx08	1255.60	101.36	79.40
Dx09	1334.88	100.58	80.80

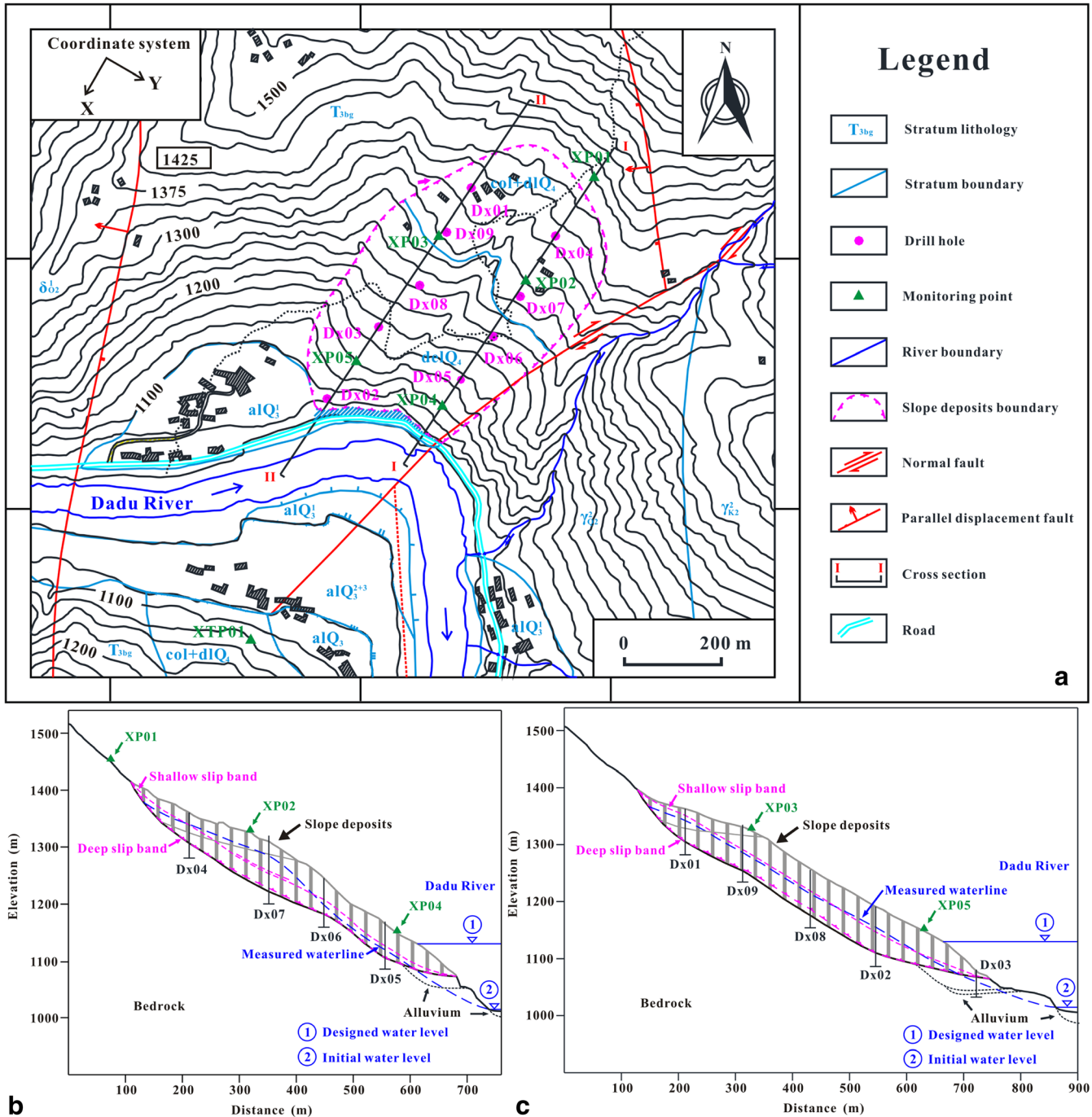


Fig. 3 Geological conditions of the Xinhua slope: **a** topographic map of the Xinhua slope, **b** cross section I-I, and **c** cross section II-II. Keys of rock stratum: T_{3bg} is the sandstone and shale of the Baiguowan group of the Triassic system; $\delta_{O_2}^3$ is the quartz diorite; $\gamma_{K_2}^2$ is the syenogranite; $\gamma_{Q_2}^2$ is the quartz monzonite and quartz granite; alQ is the alluvium in first terrace; alQ_3^{2+3} is the alluvium in second terrace; alQ_3^1 is the alluvium in third terrace; $col + dlQ_4$ is the colluvium; and $delQ_4$ is the ancient landslide deposits

deposits, and the river terrace are characterized by floated pebble gravel (alQ_3^1) with high psephicity.

Figure 3a also shows that the deposits of Xinhua slope are located between the east and the west branch of the Dadu normal fault, a region with the formation of an active structure. The distance between the west branch fault and the upstream side is

approximately 450–600 m, and the distance between the east branch fault and the downstream side is approximately 100–200 m. Furthermore, a piece of parallel displacement fault behind the downstream side is developed with a similar direction as the slope deposits distribution and the strike of $N60^\circ E$. The sandstone contains three groups of major joints in the reservoir area, a group

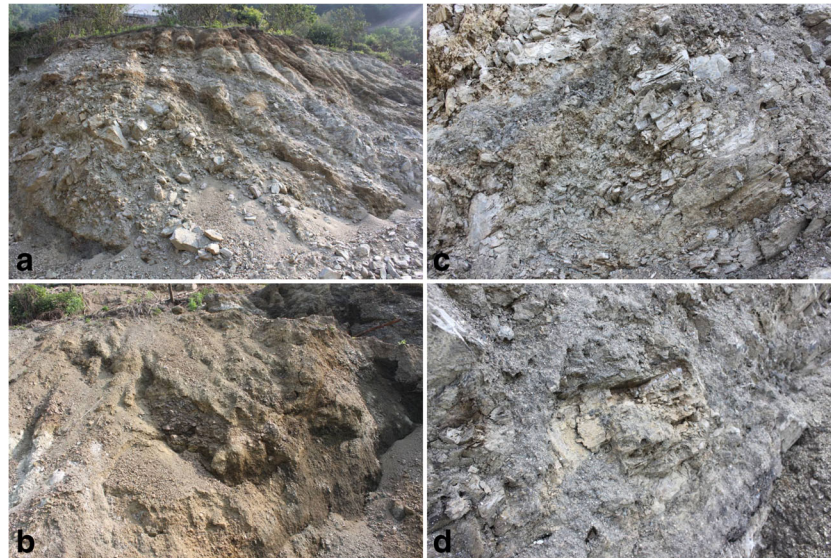


Fig. 4 Rock-soil compositions exposed on the Xinhua slope: **a** and **b** are two site photos exhibiting the ancient landslide deposits; **c** and **d** are two site photos exhibiting the shallow strongly weathered and fractured rock masses

of which is developed with the same dip direction as the slope inclination.

Hydrology

The Dagangshan reservoir is located in a mountain valley area with daily regulation of the water level. Figure 5 shows the rainfall and fluctuation of the water level for the Dagangshan reservoir. The water level of the reservoir fluctuates no more than 10 m. The normal water level of the Dagangshan reservoir is 1130 m and the static water level is 1120 m (Fig. 5b). There are two meteorological stations in the Dagangshan reservoir area. The Luding meteorological station is approximately 72 km away in the upstream of Dadu River, and the Shimian meteorological station has the approximate distance of 40 km from the downstream. The elevations of these two meteorological stations are 1321.2 and 874.3 m, respectively. The major part of the Dadu River basin is located in the transition zone between the Qinghai-Tibet Plateau and the Sichuan Basin, where the complicated topography causes a great difference of basin climate. If following the climatic regionalization, the upstream of Dadu River has the plateau climate and the middle and lower reach of subtropical moist climates. A unique vertical mountain climate has been formed in reservoir area, affected by southeast and southwest monsoons and cold air of the Qinghai-Tibet Plateau. According to statistical analyses of the data from the meteorological stations, the Dagangshan reservoir belongs to the plateau climate zone in the west of Sichuan Province. The Dagangshan reservoir has mean annual precipitation of over

600 mm. The occurrence of rainfall is concentrated between June and September when the percentage of precipitation is between 70 and 80% (Fig. 5a). In summer, there is the frequent occurrence of torrential rain in local areas with short duration, high intensity, local distribution, and the maximum amount of daily precipitation over 100 mm.

In the river basin, the primary source of runoff comes from atmospheric precipitation and secondary supplies are ice and snow melt water and ground water. As is known from the hydrological records in the Luding meteorological station during the years from 1952 to 2003, the annual mean flow rate is approximately 891 m³/s. The change rule of runoff is consistent with the precipitation that the evolution patterns for each year are similar but the variations in a year are significant. The runoff is concentrated in the flood season and the percentage during the period from May to October is approximately 81.1% of annual runoff.

Cracking and failure of the slope

In this section, the typical failure phenomena of the Xinhua slope after reservoir impoundment are described and analyzed using the results from UAV and field investigations.

Cracks among the slope surface

Field investigation during the construction process of the Dagangshan hydropower station revealed that there were several ground cracks distributed on the gentler upper slope at the

Table 2 Mechanical properties of slope deposits in different zones

Location	Natural state Cohesion (kPa)	Internal friction angle (°)	Saturation state Cohesion (kPa)	Internal friction angle (°)
Zone I	27.0	29.0	20.5	27.5
Zone II	54.0	24.0	38.0	20.5
Zone III	22.8	28.0	21.0	26.5

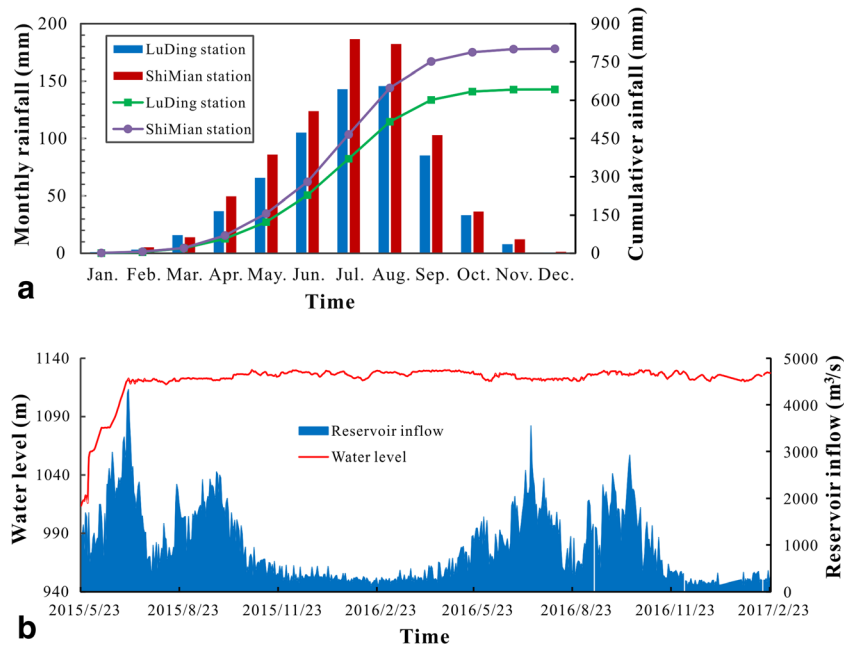


Fig. 5 Rainfall and fluctuation of the water level for the Dagangshan reservoir: **a** Hydrological records from two meteorological stations (the data is mean annual values) and **b** impoundment and water level variation of the Dagangshan reservoir

approximate elevations of 1290, 1335, and 1410 m, which were the result of the long-term unloading of slope deposits (Table 3). The early deformation behavior and borehole data provide a basis for the finding that the Xinhua slope was always in a critical state between stability and activity.

Since the reservoir impoundment on 29 May 2015, continuous inspection and observation work were conducted. There are six ground cracks with slow growth in length distributed along the border of zone II and zone I. The reservoir came to a termination elevation of 1120 m in the impoundment process in early July 2015 and the width measurement for these cracks (L1–L6) was done during the first half of July. Although these cracks have a length of approximately 1.10–3.85 m (Table 3), there was no indication of a tendency for increasing growth. Meanwhile, since the middle of July, a series of new cracks (K1–1–K12–1) were gradually found to exist around the border, especially those causing severe shear-tension deformation and settlement on the mountain roads (as shown in Fig. 6). Therefore, another measurement and investigation of these new-found cracks was executed during the second half of July (Table 4). These new-found cracks had a length of 1.02–3.29 m on July 31, an average increment speed of 0–0.078 m/day, with a maximum of 0.008–0.151 m/day during the observation period.

Significant morphological changes, especially of the mountain roads, were observed between the two field investigation times (Fig. 6). In the area covered by slope deposits, the cracks at the outside edge exhibit shearing deformation with ground surface settlement in continuous growth. The settlement value of a shear crack was around 0.4 m on 30 July 2015. By 10 August 2015, the settlement value had increased to approximately 1.0 m with the lower side of the surface in a fractured state. However, the majority of the cracks inside the covering area of slope deposits initially exhibit tension deformation, such as the example presented by

Fig. 6a. From 30 July to 10 August with the acceleration of creep movement in the Xinhua slope, the deformation behavior of the tension cracks increasingly expressed evident tension-shear failure.

Collapse and shallow failure

There are two types of collapse and/or failure that appeared in the Xinhua slope. The first type is small-scale shallow failures on the ground surface in a local region, of which the occurrence is increasingly frequent in the heavy rainfall season. As shown in Fig. 7, small-scale shallow failures around the mountain road (region A) occurred following the heavy rain in early July. The combination of intense rainfall and the free surface of the road cut and the loose structure and weak shear strength of the shallow slope deposits most likely facilitated failure.

The second type is toe-erosion collapse along the river bank. On 18 July 2015, the reservoir had just achieved the 1120-m impoundment (Fig. 8a). There were a series of deformation with the formation of concave structures near the river bank. These recesses are labeled #1, #2, and #3 in order. The #1 recess is located in region B and belongs to the upstream face of the wedge slope. The #2 recess and #3 recess are situated in region A. The #2 recess belongs to the flat surface beside the ridge and the #3 recess is shaped at the ridge. With observation of the deformation on 30 July 2015 (Fig. 8b), a new recess labeled #4 was shaped at the ridge of the wedge slope in region B. The other existing recesses experienced successive collapse and continuous development until 10 August 2015 (Fig. 8c). The recesses at the ridge (#3 and #4) have morphological changes of enlarging to the surrounding area in succession, and the recesses in the upstream surface (#1 and #2) stretch its enlargement to two sides along the bank line. However, the #1 and #4 were integrated into a new formation. However, from Fig. 8d, it can be found that the velocity of development was set to

Table 3 Pre-existing cracks measured during July 1–15 on the surface of the Xinhua slope

Mark number of cracks	L1 L1-1	L2 L2-1	L2-1	L2-3	L2-4	L3 L3-1	L3-2	L3-3	L4 L4-1	L4-2	L4-3	L4-4	L5 L5-1	L6 L6-1	L6-2
Length (m)	2.06	1.33	1.79	1.10	1.40	1.85	2.85	1.95	2.61	3.70	1.35	1.37	1.11	3.85	3.01

slow and only a series of small collapses had occurred along the shore line on 13 July 2016.

Methods

The operation of deformation monitoring in the Xinhua slope is carried out with the GNSS automatic monitoring system (Biagi et al. 2016), including a satellite positioning reference station with continuous operation and five deformation monitoring points as shown in Fig. 3a. There are two GNSS monitoring cross sections assigned for the Xinhua slope. The GNSS reference marked by XTPo1 is built on the stable bedrock of the opposite bank. As shown in Fig. 3, three monitoring points are placed in an I-I cross section at the elevations of 1150 (XPo4), 1325 (XPo2), and 1450 m (XPo1), respectively (Fig. 3b), and the other two monitoring points are installed in II-II cross section at the elevations of 1150 (XPo5) and 1325 m (XPo3), respectively (Fig. 3c. For better analyses of the monitoring data, a 3D coordinate system has been employed. The normal direction of cross sections is defined as Y-direction, and a horizontal direction perpendicular to the normal direction is defined as X-direction. The direction from XPo1 to XPo4 is positive in X-direction and the direction pointing to downstream is positive in Y-direction. The Z-direction is vertical direction and the direction to down is positive. The COSAGPS software is used for accuracy estimate of GPS coordinate in all monitoring points and the results show that the precision of X-direction coordinate is 0.1 mm, the precision of Y-direction coordinate 0.4 mm, and the precision of Z-direction 0.2 mm (Shi et al. 2015).

Analyses of slope deformation

Real-time monitoring has been performed for an accurate understanding of the deformation of the Xinhua slope. The whole monitoring history is from 23 May 2015 to 23 February 2017. The recent occurrence of great earthquake in this area is the April 20, 2013 Lushan earthquake (Mw 7.0), which is approximately 100 km away from the Xinhua slope. There is no occurrence of moderate-to-strong earthquake larger than Mw 4.0 in the surrounding area since the start of reservoir impoundment. Therefore, for the Xinhua slope, the influence of seismic load on the slope deposits is very small. During this period, the time evolution of cumulative displacement and reservoir water level are shown in Fig. 10. Some meaningful phenomena are observed as follows.

Response time delay

As shown in Fig. 9, the initial response of deposits in the Xinhua slope was a discharge from microscopic negative displacement to positive. In the first few days, the negative displacement was induced by the absorption of water at the lower slope deposits, owing to the loose accumulation and the softening of a few argillaceous rocks. The cumulative negative displacements of slope deposits were no more than 4.0 mm, and the increasing trend was abruptly stopped since the following slipping/creep deformations.

After the water level reaching 1120 m, the initial response of the slope deposits had an obvious delay comparing with the rising of the water level (Fig. 9b). The data from the monitoring points highlight that the time interval between the ending moment of impoundment and the starting moment of extension deformation are 14, 7, 12, 4, and 2 days for monitoring points XPo1, XPo2, XPo3,

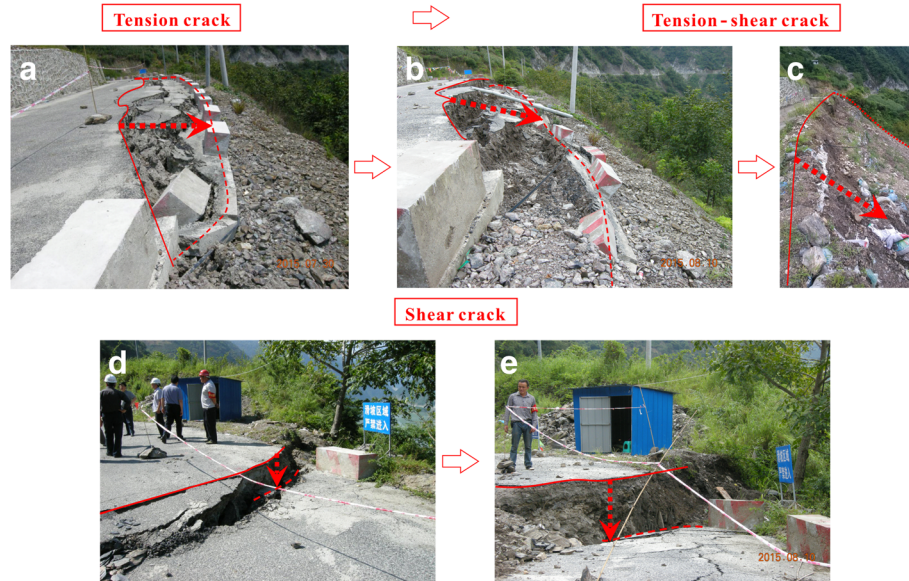


Fig. 6 Damage to a mountain road from ground cracks in region B: a and d are taken on 30 July 2015; b and e are taken on 10 August 2015; c is taken on 13 July 2016

XPo4, and XPo5, respectively. These time intervals are called the response time. It can be seen that the length of the response time is relevant to the location of the monitoring point, where points closer to the river bank have lower response time. It is unreasonable to consider the occurrence of extension deformation in different locations as simultaneous events. Therefore, the complex phenomena show that the deformation of the Xinhua slope is under progressive failure with the tendency of sacrificing the lower part for development.

Spatial variation

During the monitoring process, all monitoring sites were in operation, except for XPo5, which slide into the water on 9 August 2015. The immediate recorded value of cumulative displacement (3.3 m) in X-direction was much less than the horizontal distance (36.2 m) from the river bank, which indicates that the movement of the slope deformation is not characterized by the overall instability of rock mass or interconnected rock blocks.

As shown in Fig. 10 and Table 5, the deformation has different performances in different directions and different locations. The points in region B had more active performance than those in region A. In the X- and the Z-directions, the phenomenon can be found from the evolution of cumulative displacement (Fig. 10), which indicates that the deformation in the location of the monitoring points appears as a negative correlation with the distance from the river bank. Meanwhile, the cumulative displacement in the X-direction is generally higher than that on the Z-direction. However, the Y-direction was showing deformation of different development and distribution. The points XPo2 and XPo3 are closer to the river bank, but the cumulative displacements in the Y-direction are less than the point XPo1, which indicated that zone II is stable in the Y-direction. Regarding the spatial dimension, the horizontal deformation of the points XPo2 and XPo3 has a concentrated expression in the X-direction.

Since 22 July 2015, the deformations at different positions became in synchronous response, with a high increasing velocity of

accumulative displacements. As shown in Fig. 8 and Table 4, there were persistent occurrences of toe-erosion collapse in front edge of slope deposits and an increasing trend of new-found crack length at the same time. In the next few days, all the points were slipping closer to the river bank at the average speed of 27.4, 39.9, 36.3, and 94.3 mm/day in the X-direction for the monitoring points XPo1, XPo2, XPo3, and XPo4, respectively. There was the fastest growth of accumulative displacements occurring in the whole monitoring period. At the end of November, the project of water level to 1130 m was finished. Before that time, the increasing velocity of accumulative displacement was gradually slowing down, which stated that the slope deposits had increasingly adapted to the new water level by means of slip/creep movement and morphological transformation.

Time variation

As shown in Fig. 11, there is a dynamic process of deformation during the next period. Taking an example of the monitoring points XPo1 and XPo4, three time slots are adopted as typically representative to explain the adverse factors influencing slope deformation. There was a strong correlation between the cumulative displacement and the change of water level from time slot A (from 29 October to 9 December 2015). The fluctuations of water level were found to relate to the variation of deformation velocity. When drawdown of water level was occurring, there was an immediate increasing of accumulative displacement. However, when the subsequent rising of water level was happening, the increasing velocity was immediately decreased. However, the deformation pattern is not constantly valid for the whole monitoring period.

During the time slot B (from 23 February to 8 June 2016), there was a different response: all the locations in the slope deposits had almost no creep no matter how the water level changes. The growth of cumulative displacement stopped, but the value of velocity had strong fluctuation around the zero line when the water level decreased. In contrast, the extent of the fluctuation was weakened when the water level increased. Considering the

Table 4 The characteristics of new-found cracks measured during July 16–31 on the surface of Xinhua slope after reservoir impoundment

Mark number of cracks	K1-1	K2-1	K2-2	K3-1	K3-2	K3-3	K4-1	K4-2	K5-1	K6-1	k6-2	K7-1	K8-1	K9-1	K10-1	K11-1	K12-1
Length (m)																	
July 16	0.89	1.07	1.79	0.75	1.38		0.93		1.18	1.10		1.23	1.18				
July 17	0.90	1.07	1.81	0.75	1.39		0.93		1.18	1.11		1.24	1.19				
July 18	0.91	1.08	1.82	0.75	1.40		0.94		1.19	1.11		1.25	1.19				
July 19	0.93	1.08	1.84	0.75	1.42		0.95		1.20	1.12		1.26	1.20				
July 20	0.96	1.09	1.87	0.76	1.45		0.97		1.22	1.09		1.27	1.21				
July 21	0.99	1.11	1.90	0.77	1.47		0.98		1.23	1.10		1.29	1.23	1.07	1.04	0.96	1.55
July 22	1.03	1.13	1.94	0.79	1.50		1.00		1.23	1.10		1.30	1.24	1.08	1.04	0.96	1.57
July 23	1.08	1.16	1.99	0.81	1.54		1.03		1.23	1.09		1.32	1.27	1.08	1.05	0.97	1.60
July 24	1.13	1.19	2.00	0.83	1.54		1.05		1.33	1.09		1.34	1.29	1.09	1.06	0.97	1.63
July 25	1.19	1.22	2.09	0.87	1.54		1.07		1.29	1.09		1.36	1.32	1.09	1.06	0.98	1.67
July 26	1.27	1.28	2.17	0.92	1.56	2.90	1.11	2.37	1.34	1.09	1.95	1.40	1.36	1.10	1.07	0.98	1.73
July 27	1.36	1.32	2.25	0.96	1.60	2.98	1.14	2.42	1.39	1.08	1.99	1.43	1.41	1.10	1.08	0.99	1.78
July 28	1.40	1.39	2.36	1.03	1.65	3.07	1.18	2.48	1.45	1.09	2.02	1.48	1.47	1.11	1.09	1.00	1.82
July 29	1.55	1.45	2.42	1.06	1.70	3.13	1.22	2.52	1.49	1.09	2.07	1.52	1.52	1.11	1.11	1.01	1.89
July 30	1.64	1.50	2.52	1.10	1.74	3.21	1.27	2.58	1.93	1.09	2.10	1.56	1.57	1.12	1.12	1.01	1.92
July 31	1.74	1.55	2.6	1.14	1.78	3.29	1.33	2.65	1.99	1.10	2.16	1.61	1.63	1.13	1.13	1.02	1.99
Average	0.057	0.032	0.054	0.026	0.026	0.078	0.027	0.055	0.054	0	0.042	0.025	0.030	0.006	0.009	0.007	0.045
Max	0.151	0.069	0.105	0.068	0.049	0.091	0.058	0.069	0.438	0.008	0.056	0.048	0.057	0.012	0.022	0.012	0.075
Increment speed (m/day)																	

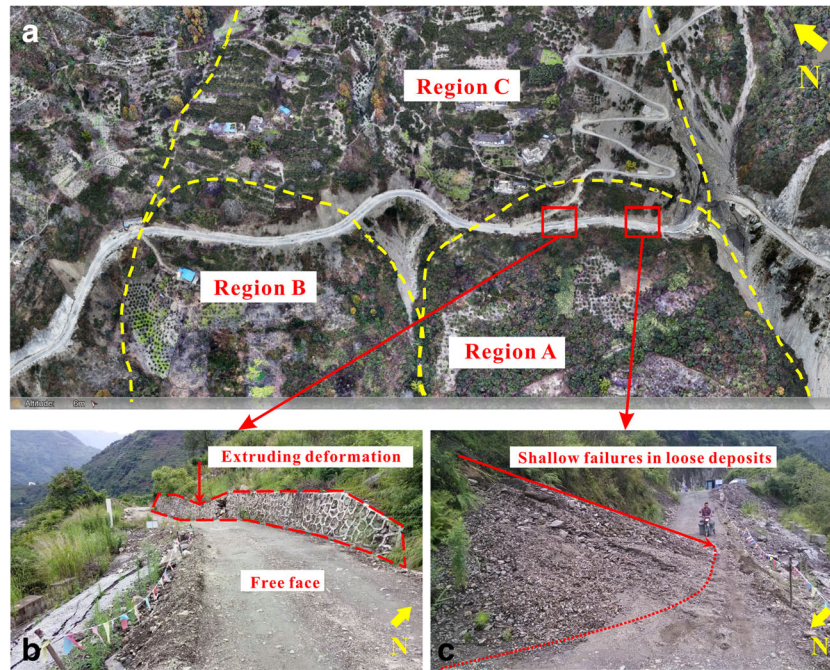


Fig. 7 Shallow failures around the mountain road in region A due to the heavy rain in early July: **a** oblique photography by the UAV, **b** the first shallow failure, and **c** the second shallow failure blocking the road

time slot C (from 16 June to 21 September 2016), the deformation pattern turned out to be the same as the time slot A. In almost a year, there had been two kinds of responses to the fluctuation of water levels illustrating that the deformation of slope deposits is very complex, involving many factors. The factor causing the response of slope deposits is the fluctuation

of water levels, but the difference between two kinds of response may be caused by floods, intense rainfall, and high reservoir inflow in detail.

The normal flood season of the Dadu River is from around the end of June to the beginning of September. As shown in Fig. 5, there was a dramatic increase of rainfall and reservoir inflow in

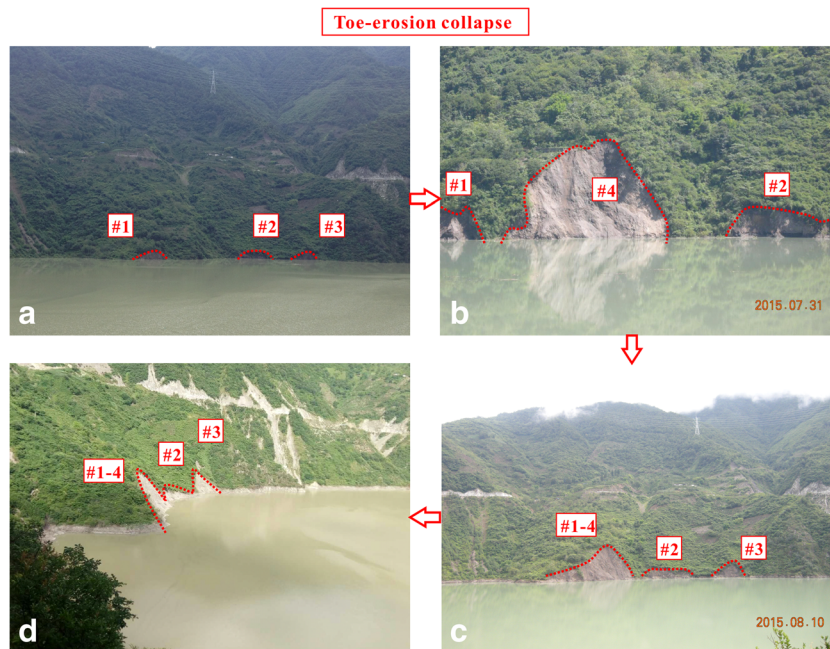


Fig. 8 Toe-erosion collapses along the bank toe at different times: **a** was taken at the finishing time of the impoundment process, **b** was taken on 31 July 2015, **c** was taken on 10 August 2015, and **d** was taken on 13 July 2016

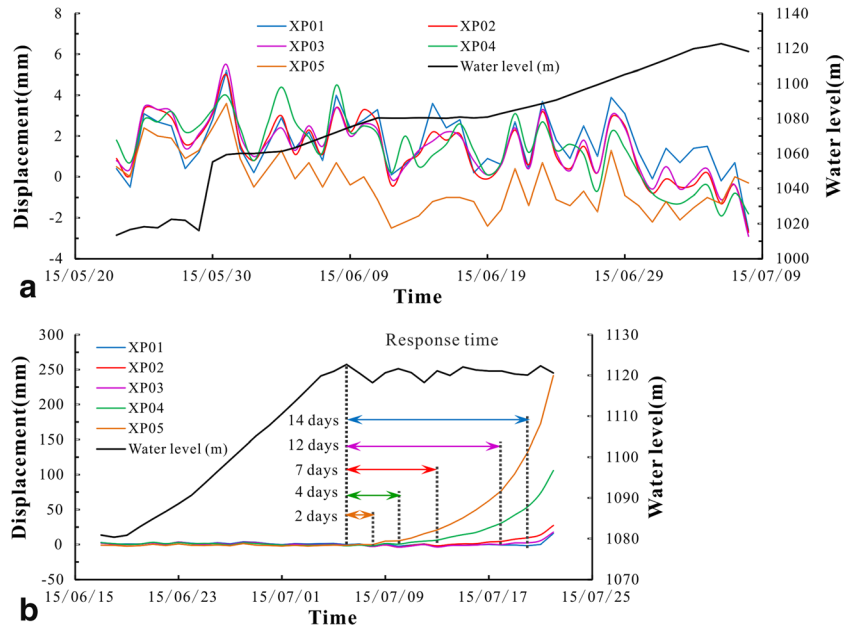


Fig. 9 Initiation of the deformation process for the slope deposits in the Xinhua slope after the impoundment: **a** negative displacement during the impound period (X-direction displacement as an example) and **b** difference of response time after impoundment

flood season. As shown in Fig. 11, time slots A and C were in flood season but time slot B was in the hydraulic condition with little rainfall and low reservoir inflow. After 28 November 2016, the

Dadu River started to enter the dry reason and the slope deposits had the same response law to the fluctuation of water level as time slot B.

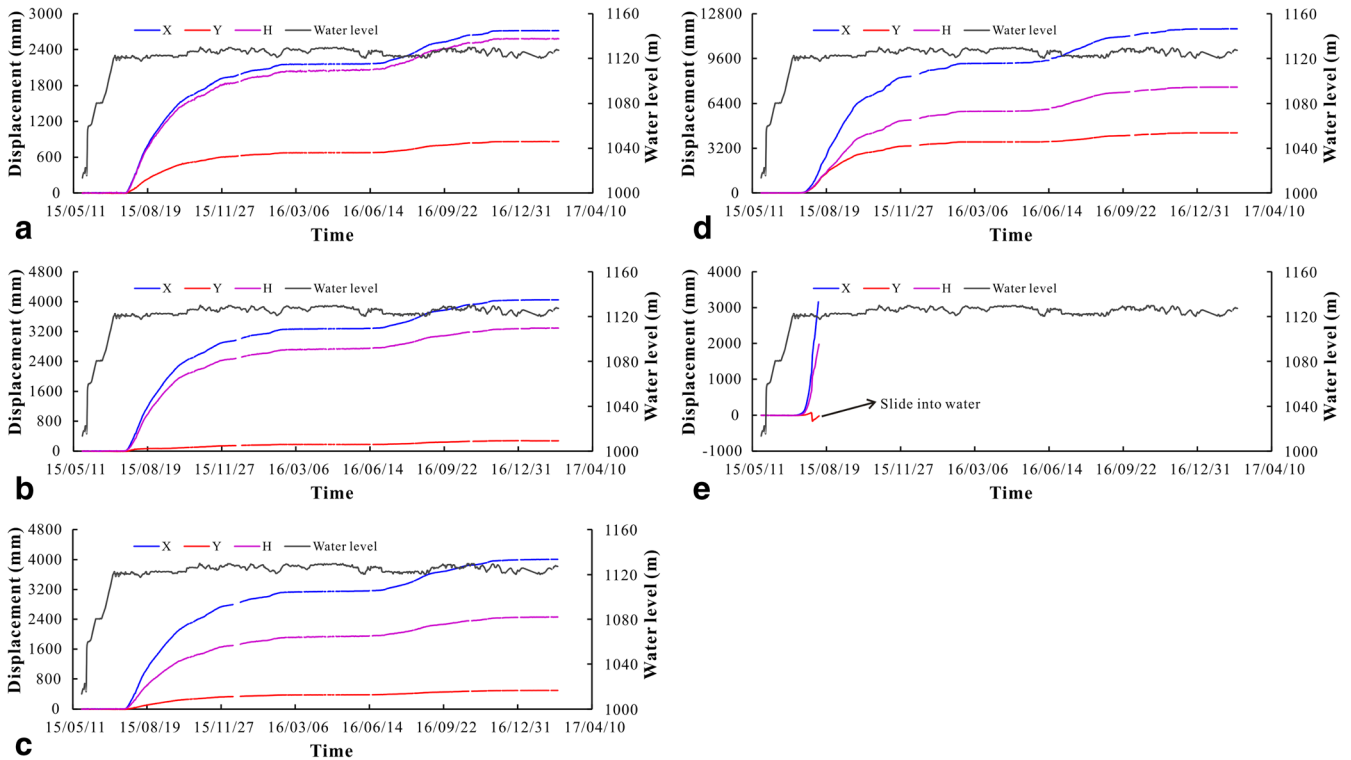


Fig. 10 Time evolution of cumulative displacement in different directions for different monitoring points: **a** monitoring point XP01, **b** monitoring point XP02, **c** monitoring point XP03, **d** monitoring point XP04, and **e** monitoring point XP05

Table 5 Deformation features during the monitoring period on October 10, 2016 (due to sliding into the water, the deformation data for point XP05 disappeared on August 9th, 2015)

Monitoring point	Cumulative displacement (mm)			Horizontal distance from river bank at 1130 m (m)
	X-direction	Y-direction	Z-direction	
XP01	2715.8	862.8	2849.6	538.4
XP02	4050.5	275.9	3290.0	290.7
XP03	4009.6	500.2	2461.7	337.6
XP04	11,717.7	4302.6	7573.1	37.7
XP05	3305.3	-17.1	1977.8	36.2

Discussions

The field investigations and 2-year monitoring results yield a full record of the deformation characteristics of the deposits in Xinhua slope. The identification of an ancient landslide confirms the existence of basic conditions for sliding, including the slip mass, slip surface, and slip bands (deep and shallow layers). The slope deposits, seen as the loose debris accumulations that are sensitive to aquatic action, have the main composition of crushed stone and silty clay. As an example of gravitational geologic hazards, the slope deposits of zones II and III become the subject of the movement process. In fact, the mechanical and morphological relationships are difficult to define precisely between the slope deposits of zones II and III. Based on these sliding conditions, it is possible to undertake stability analysis and mechanism discussion for the Xinhua slope. However, there is a diversity of deformation features in the face of external environmental changes as shown from the above description and summary.

Impoundment

According to the slope classification by elevation, the Xinhua slope is a high slope with rock and soil deposits above the original water

level of the Dadu River. Since the initial impoundment with 100-m increase of water level, the reservoir has covered the lower part of the slope deposits (Figs. 3 and 8). Figure 10 indicates that the change of water level resulted in the destabilization of the identified landslide.

The stability of slope had been reduced significantly after a large-scale rising of water level (Ji et al. 2005). This phenomenon can be explained by three possible reasons. First, the abrupt and substantial increase of water level promoted a large volume of slope deposits to change the saturated state with the uplift of the groundwater table and the range extension of the phreatic aquifer (Tu et al. 2011). There was transient seepage forming in slope deposits owing that the uplift of the groundwater table lagged behind the uplift of water level. Due to the transient seepage and the softening and argillization with invasion of reservoir water, the mechanical strength of slip soils was decreased, which cause that the deteriorated shear resistance along the slip surface made an increasing trend of sliding downward. Second, although seepage force and increased external hydrostatic pressure by uplift of water level were in favor of slope stability (Okeke and Wang 2016), some adverse changes mechanical behavior produced considerable

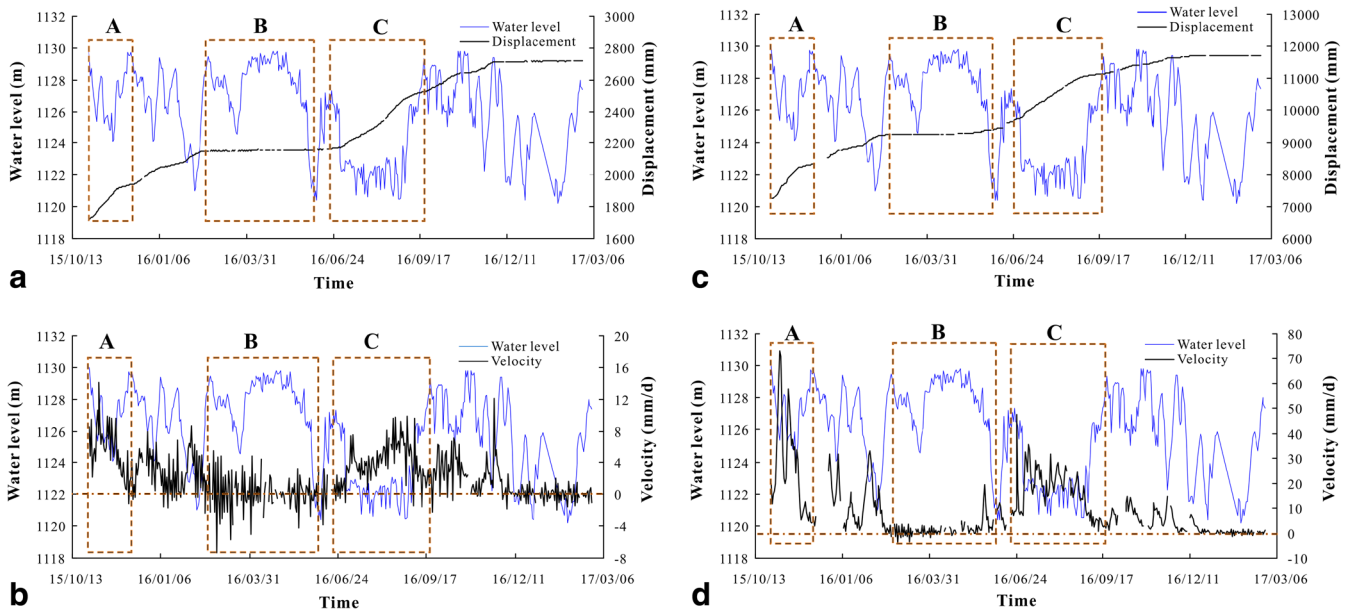


Fig. 11 Comparison of deformation performance under different conditions of the water level drawdown: **a** cumulative displacement of monitoring point XP01, **b** deformation velocity of monitoring point XP01, **c** cumulative displacement of monitoring point XP04, and **d** deformation velocity of monitoring point XP04 (A is a time slot from 29 October to 9 December 2015; B is a time slot from 23 February to 8 June 2016, and C is a time slot from 16 June to 21 September 2016)

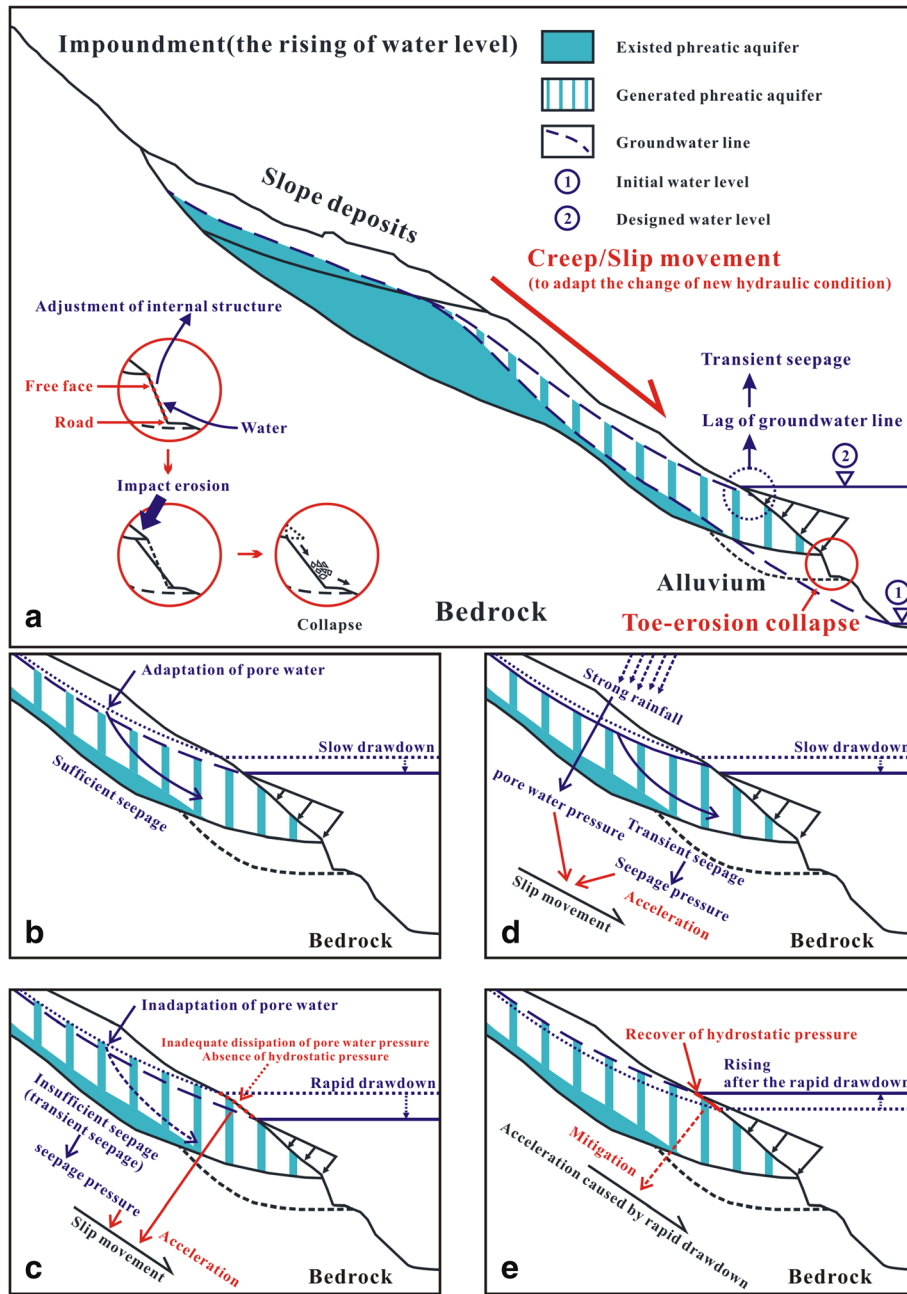


Fig. 12 Response mechanism of the Xinhua slope due to reservoir impoundment and rainfall: a impoundment stage and cases in operation stage, b slow drawdown of water level, c rapid drawdown of water level, d slow drawdown of water level with strong rainfall, and e raising of water level after rapid drawdown

harm to the stability of slope deposits, including the pore water force and the decreased slip resistance. The increased pore water pressure along the slip surface was caused by the extension of the phreatic aquifer. Then, the increase of water content generated the buoyancy force on the lowest part of slope deposits and further reduced the slip resistance force. Third, the excavation and construction of mountain roads undercut the toe of slope deposits and created an adverse condition for its stability. After the impoundment, the free face and foot part of the slope deposits were completely exposed in the water which subsequently suffer the action of water erosion, current impact, and enhanced slip force. The adverse condition of long term made mechanical strength of

slope toe region decreased and further caused the inability of storing pore water and maintaining pore water pressure. When sufficient soaking lead to the instability, the toe region of slope deposits generated collapse failure that created space for the creep/slip movement of the inner slope. Subsequently, the retained slope deposits had a tendency to slide into the water and the toe collapse has a persistent development along the slip surface (Fig. 8).

Fluctuation of the reservoir water level

From the above monitoring analyses, it is already known that the drawdown of the water level after impoundment accelerated the negative effects on slope stability. However, there is a reflection

from the falling rate of the water level into the deformation response of the slope deposits. As shown in Fig. 12b, the pore water inside the slope deposits has a strong adaptability to the slow drawdown of water level. When water level was made a slow decrease, the falling of groundwater table surface can follow the slow decrease with time. Due to fully outflow of pore water, there was no transient seepage appearing inside slope deposits with the timely dissipation of pore water pressure. In this situation, the slope deposits maintain a relatively stable. However, if there is a rapid drawdown as shown in Fig. 12c the pore water of slope deposits will show an inadaptability response. Due to the deficient outflow of pore water, the range of the phreatic layer was reduced from before but kept a relatively large scale, causing the transient seepage inside the part above water level of the slope deposits (Bansal and Das 2011). Next, the rapid flow of groundwater took away fine particles of slip soils with erosion effect made slope deposits more loose and further reduce the slip resistance. From the point of mechanical response, the phreatic layer of large scale cause that the dissipation of pore water pressure lagged behind the decrease of external hydrostatic pressure (Okeke and Wang 2016). Meanwhile, the transient seepage inside slope deposits made seepage force along the slip direction. Ultimately, the mechanical disadvantages turned into the acceleration of the creep/slip movement.

Except for the rising of reservoir water level during the impoundment period, the later rising must be immediately followed by the drawdown with the design limit of the water level. As shown in Fig. 11, if there had been a rapid drawdown before, the subsequent rising had a mitigation effect on the movement acceleration caused by the rapid drawdown. When the water level decreases to the design water level, the reverse seepage of reservoir water weakens the osmotic pressure and recovers the hydrostatic pressure, which is represented as the convergence of cumulative displacement.

Flood season

As shown in Figs. 11 and 12, the standard definition for the declining speed of a reservoir water level is impossible to remain constant. The identification depends on the stability and adequacy of the seepage inside the slope deposits. During the rainfall infiltration, the water streams made cemented material dissolved and enhanced lubrication action between particles and further promoted the migration and loss of fine particles in slip soils. When suffering the frequent fluctuation of the water level, the much loss of fine particles made pores of slope deposits interconnected and forming seepage channels. Meanwhile, a gradual expansion of seepage channels improved slope deposits' adaptive capacity for the changing of water level. Time slot B in Fig. 11 shows that the drawdown within a certain range of decline speeds makes almost no difference on the cumulative displacement, but the active degree in the critical state is improved and is related with declining speed.

However, the influences of river water on the deformation process of the slope deposits are complicated and complex. It can be found that intense rainfall infiltration is an adverse factor for the seepage process from the diverse response in time slot C. In the flood season, there is often heavy rainfall and accelerated reservoir currents. The invasion of large volumes of rainwater has an elevating effect on the groundwater surface table (Tiwari and Lewis 2014). The high-velocity reservoir currents enhance

erosion and impact. When the subsequent slow drawdown of the water level is happening, the lifted groundwater surface table delays the outflow of pore water. Transient seepage flow is presented again with the action of deficient seepage and the enhancement of pore pressure, which is similar to the adverse consequence caused by the rapid drawdown of the water level. Therefore, the flood season is considered to lower the identification standard for rapid drawdown, which endangers the slope stability.

Conclusions

Geomorphology and subsurface investigations show that the accumulated deposits in Xinhua slope are primarily identified as ancient landslide deposits at high altitude in the Dagangshan reservoir. There is a geological response from 2 years of monitoring and observation since the reservoir impoundment on 29 May 2015. The deformation features and monitoring analysis highlight that the slope deformation after impoundment is mainly progressive slope failure, identified as the reactivation of an ancient landslide. During the whole monitoring period, there was no occurrence of seismic loading. The failure in the Xinhua slope is considered as a progressive dynamic process beginning with toe erosion, the development of rear cracks, and the persistence of front collapse. The groundwater seepage field is the most critical step for understanding the deformation behavior of slope deposits. The monitoring analysis recognizes three main factors that accelerate the deformation velocity of slope deposits: the initial impoundment, the rapid drawdown of the water level, and the attendance of flood season. The three adverse factors influence the movement of seepage flow inside the slope deposits and further change the internal mechanical and physical properties. The 1963 Vaiont landslide has been always concerned as a representative reservoir disaster causing irreparable painful consequences (Semenza and Ghirelli 2000). If comparing Vaiont landslide and the deformation of slope deposits in Xinhua slope, some similar places can be found: the reactivation of ancient landslide, influenced by artificial excavation, and suffering the influences from impoundment, fluctuation of reservoir level, and rainfall. However, a significant difference also existed that a weak intercalation characterized by clay was present along the slip surface in Vaiont ancient landslide. Eventually, twice impoundments and intense rainfall generated the landslide disaster. However, in Xinhua slope, the impoundment was not enough to make a landslide happening there but a large deformation.

The slip/creep movement of slope deposits is triggered by complicated and complex hydrological changes and not simply a disadvantage factor. There were two instances of large deformation that occurred during the whole monitoring process, which can explain how the disadvantage factors influence slope deposits' stability. The first one came in July 2015 and lasted at least 7 months, ending with the convergence of cumulative displacement. The next one had an operation process of approximately 5 months with the beginning in July 2016. The most serious influence on the Xinhua slope was derived from the large-scale rising of the water level in the impoundment period. Exactly, the unfavorable consequence can be assumed to be the integration of the 100-m rising water levels and flood season participation. This large deformation was initiated in the slope foot and created the deformation space of the latter parts. In this period, the slope toe region suffers adverse performance from the strong currents from increasing runoff in the flood season with the action of scour and erosion and the secondary consequence of softening and collapse.

However, as shown in Fig. 8, the adverse effect from the impoundment is not enough to make the overall instability of slope deposits and ultimately lead to the lowest part sliding into water. Furthermore, as shown in Fig. 10, the increase of accumulative displacement had gradually slowed down and finally even almost stopped before the second large deformation with the dry season coming.

The subsequent large deformation starting in July 2016 is characterized by the integration of the drawdown of water level and the flood season. The Dagangshan reservoir water level is regulated daily with a maximum fluctuation of no more than 10 m. In any case, the evident displacement is difficult to observe and measure when the slope deposits have adapted to the normal water level of 1130 m, except that the flood season gets involved in the instability framework. That phenomenon is observed because the adverse effect caused by the drawdown of the water level in dry season is insufficient to trigger the instability framework. As shown in the monitoring analysis, the flood season took effect by invading the slope surface with transient seepage flow and the following drawdown of the water level aggravated the instability of the unstable seepage.

River sediment is one of the major threats for hydraulic and hydroelectric engineering. When water flow into a reservoir, a higher water depth with the rising of reservoir level will reduce flow velocity of flow and promote sediment deposition. If a large amount of sediments deposit in reservoir, the effective storage capacity will be reduced and unfavorable to the reservoir. For the reservoir operation, the outlet structure is normally used for discharging flood and sediment when in flood season of large flow and sediment runoff. Therefore, sediment ejection and flood discharge are indispensable engineering actions that are executed by rapid drawdown of water level in flood season. A method to complete these actions becomes the key to controlling the deformation of slope deposits. Improving the efficiency of discharging sediment for outlet structure and strengthening seepage ability of slope deposits are possible consideration for reducing the slope instability risk. These approaches can be achieved by constructing soil and water conservation engineer in upstream of dam site and drainage works in Xinhua slope.

Acknowledgements

Critical comments by the anonymous reviewers greatly improved the initial manuscript.

Funding information

We gratefully acknowledge the support of the National Natural Science Foundation of China (41472272) and the Youth Science and Technology Fund of Sichuan Province (2016JQ0011).

References

Bansal RK, Das SK (2011) Response of an unconfined sloping aquifer to constant recharge and seepage from the stream of varying water level. *Water Resour Manag* 25(3):893–911. <https://doi.org/10.1007/s11269-010-9732-7>

Berilgen MM (2007) Investigation of stability of slopes under drawdown conditions. *Comput Geotech* 34(2):81–91. <https://doi.org/10.1016/j.compgeo.2006.10.004>

Biagi L, Grec FC, Negretti M (2016) Low-cost GNSS receivers for local monitoring: experimental simulation, and analysis of displacements. *Sensors* 16(12):2140. <https://doi.org/10.3390/s16122140>

Bjerrum L (1967) Progressive failure in slope of overconsolidated plastic clay and clay shales. *Terzaghi Lect* 2:77–78

Casagli N, Frodella W, Morelli S, Tofani V, Ciampalini A, Intrieri E, Raspini F, Rossi G, Tanteri L, Lu P (2017a) Spaceborne, UAV and ground-based remote sensing

techniques for landslide mapping, monitoring and early warning. *Geoenvironmental Disasters* 4:1–23. <https://doi.org/10.1186/s40677-017-0073-1>

Casagli N, Tofani V, Morelli S, Frodella W, Ciampalini A, Raspini F, Intrieri E (2017b) Remote sensing techniques in landslide mapping and monitoring, keynote lecture. In: Mikoš M, Arbanas Ž, Yin Y, Sassa K (eds) *Advancing culture of living with landslides*, vol. 3—advances in landslide technology. Springer International Publishing, Switzerland, pp 1–19

Chelli A, Mandrone G, Truffelli G (2006) Field investigations and monitoring as tools for modelling the Rossena castle landslide (Northern Appennines, Italy). *Landslides* 3(3):252–259. <https://doi.org/10.1007/s10346-006-0046-z>

Duc DM (2013) Rainfall-triggered large landslides on 15 December 2005 in Van Canh District, Binh Dinh Province, Vietnam. *Landslides* 10(2):219–230. <https://doi.org/10.1007/s10346-012-0362-4>

Dufresne A, Prager C, Clague JJ (2015) Complex interactions of rock avalanche emplacement with fluvial sediments: field structures at the Tschirgant deposit, Austria. In: Lollino G, Giordan D, Crosta GB, Corominas J, Azzam R, Wasowski J, Scarra N (Eds) *Engineering geology for society and territory—vol. 2*, Springer International Publishing, pp. 1707–1711. doi: https://doi.org/10.1007/978-3-319-09057-3_303

Fan L, Zhang G, Li B, Tang H (2017) Deformation and failure of the Xiaochatou landslide under rapid drawdown of the reservoir water level based on centrifuge tests. *Bull Eng Geol Environ* 76(3):891–900. <https://doi.org/10.1007/s10064-016-0895-1>

Huang BL, Zheng WJ, ZZ Y, Liu GN (2015) A successful case of emergency landslide response—the Sept. 2, 2014, Shanshucao landslide, Three Gorges Reservoir, China. *Geoenvironmental Disasters* 2(1):18. <https://doi.org/10.1186/s40677-015-0026-5>

Hungr O, Leroueil S, Picarelli L (2014) The Varnes classification of landslide types, an update. *Landslides* 11(2):167–194. <https://doi.org/10.1007/s10346-013-0436-y>

Iverson RM (2000) Landslide triggering by rain infiltration. *Water Resour Res* 36(7):1897–1910. <https://doi.org/10.1029/2000WR900090>

Ji F, Shi YC, Liu HC, Deng ZW (2005) Study on formation mechanism and stability of ancient Xinhua landslide in Daduhe River. *Hydrogeol Eng Geol* 32:24–27 (in Chinese)

Okeke CU, Wang F (2016) Critical hydraulic gradients for seepage-induced failure of landslide dams. *Geoenvironmental Disasters* 3(1):9. <https://doi.org/10.1186/s40677-016-0043-z>

Panizzo A, De Girolamo P, Di Risio M, Maistri A, Petaccia A (2005) Great landslide events in Italian artificial reservoirs. *Nat Hazards Earth Syst Sci* 5(5):733–740. <https://doi.org/10.5194/nhess-5-733-2005>

Saito Y, Yang Z, Hori K (2001) The Huanghe (Yellow River) and Changjiang (Yangtze River) deltas: a review on their characteristics, evolution and sediment discharge during the Holocene. *Geomorphology* 41(2–3):219–231. [https://doi.org/10.1016/S0169-555X\(01\)00118-0](https://doi.org/10.1016/S0169-555X(01)00118-0)

Schwab JW, Geertsema M, Blais-Stevens A (2004) The Khyex River landslide of November 28, 2003, Prince Rupert British Columbia. *Canada Landslides* 1(3):243–246. <https://doi.org/10.1007/s10346-004-0026-0>

Semenza E, Ghirotti M (2000) History of the 1963 Vaiont slide: the importance of geological factors. *Bull Eng Geol Environ* 59(2):87–97. <https://doi.org/10.1007/s100640000067>

Shi J, Hua B, Chen X, Jun LI (2015) Design of GNSS automatic monitoring network of Xinhua landslide in Dagangshan reservoir area. *Yangtze River* 46:53–56 (in Chinese)

Tiwari B, Lewis A (2014) Experimental modelling of seepage in a sandy slope. In: Sassa K, Canuti P, Yin Y (Eds) *Landslide science for a safer geo-environment*, Springer, pp 109–115. https://doi.org/10.1007/978-3-319-05050-8_18

Tu GX, Deng H, Huang RQ (2011) Influence on a bank slope accumulations' stability of the rising or falling speed of a reservoir water level. *J Sichuan Univ* 42:63–70 (in Chinese)

Vandamme J, Zou QP (2013) Investigation of slope instability induced by seepage and erosion by a particle method. *Comput Geotech* 48:9–20. <https://doi.org/10.1016/j.compgeo.2012.09.009>

Wang F, Li T (2009) Landslide disaster mitigation in Three Gorges Reservoir, China. *Mt Res Dev* 30:184–185

Wang F, Miyajima M, Li T, Shan W, Fathani TF (2013) Progress of geo-disaster mitigation technology in Asia. *Environ Sci Eng* 1:565–582

Xia M, Ren GM, Ma XL (2013) Deformation and mechanism of landslide influenced by the effects of reservoir water and rainfall, Three Gorges, China. *Nat Hazards* 68(2):467–482. <https://doi.org/10.1007/s11069-013-0634-x>

Xia M, Ren GM, Zhu SS, Ma XL (2015) Relationship between landslide stability and reservoir water level variation. *Bull Eng Geol Environ* 74(3):909–917. <https://doi.org/10.1007/s10064-014-0654-0>

Yamada M, Ichikawa K, Kuwano T, Takeuchi T, Nakagawa A (2013) The interpretation for landslide mechanism and the proposal of landslide countermeasures in Abay Gorge in Ethiopia. In: Ugai K, Yagi H, Wakai A (Eds) *Earthquake-induced landslides*, Springer Berlin Heidelberg, pp. 405–406. doi: https://doi.org/10.1007/978-3-642-32238-9_42

- Yang H, Wang F (2014) Influence of water level drawdown on landslide movement in reservoir. In: Sassa K, Canuti P, Yin Y (Eds) *Landslide science for a safer Geoenvironment*, Springer, pp. 703–708. doi: https://doi.org/10.1007/978-3-319-04996-0_106
- Zhao Y, Xu M, Guo J, Zhang Q, Zhao H, Kang X, Xia Q (2015) Accumulation characteristics, mechanism, and identification of an ancient translational landslide in China. *Landslides* 12:1–12. <https://doi.org/10.1007/s10346-014-0535-4>
- Zhou JW, Xu WY, Yang XG, Shi C, Yang ZH (2010) The 28 October 1996 landslide and analysis of the stability of the current Huashiban slope at the Liangjiaren hydropower station, Southwest China. *Eng Geol* 114(1-2):45–56. <https://doi.org/10.1016/j.enggeo.2010.04.001>
- Zhou JW, Xu FG, Yang XG, Yang YC, Lu PY (2016) Comprehensive analyses of the initiation and landslide-generated wave processes of the 24 June 2015 Hongyanzi landslide at the Three Gorges Reservoir, China. *Landslides* 13(3):589–601. <https://doi.org/10.1007/s10346-016-0704-8>
- Zhou JW, Lu PY, Yang YC (2017) Reservoir landslides and its hazard effects for the hydropower station: a case study. In: Mikoš M, Arbanas Ž, Yin Y, Sassa K (eds)

Advancing culture of living with landslides, vol. 2—advances in landslide science. Springer International Publishing, Switzerland, pp 699–706

M.-l. Chen · J.-w. Zhou

State Key Laboratory of Hydraulics and Mountain River Engineering,
Sichuan University,
Chengdu, 610065, People's Republic of China
Email: jwzhou@scu.edu.cn

P.-f. Lv · X.-z. Chen

Dadu River Hydropower Development Company, Ltd.,
Chengdu, 610016, People's Republic of China

S.-l. Zhang

College of Water Resource and Hydropower,
Sichuan University,
Chengdu, 610065, People's Republic of China